Aharonov-Bohm effect in the time domain

Sara Meir, Yuval Tamir, Hamootal Duadi, Eliahu Cohen, and Moti Fridman*
Faculty of Engineering and the Institute of Nanotechnology and Advanced Materials, Bar-Ilan University, Ramat Gan, Israel

(Received 2 September 2024; accepted 5 June 2025; published 31 July 2025)

In the Aharonov-Bohm effect, charged particles accumulate a phase as they travel in space, encircling a source of magnetic flux. We develop a temporal analog of the Aharonov-Bohm effect, where the photons' path is in the time-domain instead of the spatial domain, and moreover demonstrate it experimentally with entangled photon pairs rather than single, uncorrelated quanta. Relying on the temporal SU(1,1) interferometer, the constructed interferometric scheme excels in its temporal resolution and sensitivity. This system can be applied for quantum-enhanced measurements, metrology at GHz frequencies, advanced sensing of dispersion properties, and high-precision temporal measurements.

DOI: 10.1103/3phs-9rmc

I. INTRODUCTION

In the Aharonov-Bohm effect, a charged particle accumulates a phase while it travels in space according to the vector potential along its trajectory [1–6]. Besides its fundamental importance, this effect was utilized for measuring magnetic fields [7], electron dynamics [8–10], media velocities [11], optical properties of toroidal medium [12], and optical vortices [13]. Furthermore, the effect was generalized to neutral particles [14,15], gravitational effect [16], acoustic waves [17], and photons [11,13,18–21]. In addition, the Aharonov-Bohm effect was shown when particles accumulate the phase along trajectories in domains other than the spatial one, such as the frequency [22], modal [23], and polarization [24] domains. We adapt the Aharonov-Bohm effect into the time domain, where the phase accumulates along a trajectory in time. We utilize a temporal SU(1,1) interferometer based on entangled photons traveling along different paths in the time domain [25]. Our temporal Aharonov-Bohm system allows high-resolution measurements of spatiotemporal dynamics, as well as fast phase changes in single-shot measurements with sensitivity above the shot-noise limit [25]. Beyond the interest in demonstrating this quantum effect in the time domain with entangled photons, it can be useful for quantum-enhanced measurements [26–28], metrology at GHz frequencies [29,30], advanced sensing of dispersion properties [31,32], and high-precision temporal measurements [33]. In addition, this system is sensitive to minute changes in the medium through which photons are propagating, so it might be relevant for simulating systems with fast spacetime dynamics, such as optical analogs of photon trajectories in dynamically curved spacetime [34], rotating black holes [35–38], Thomas precession [39], gravitational frame dragging [34], and red-shift effects [34].

When a wavefunction of a charged particle travels in space, it is sensitive to the vector potential in its area. Hence, the relative phase within the wavefunction can change even if the magnetic field does not reach the particle [3,40]. This lies at the heart of the Aharonov-Bohm effect and rises from the Schrödinger equation of the wavefunction, ψ, of a charged particle:

$$\frac{\partial\psi}{\partial t} = \frac{-i}{2\hbar m}\left(-i\hbar\nabla + \frac{e}{c}\mathbf{A}\right)^2\psi, \tag{1}$$

where $\mathbf{A}$ is the vector potential. The wavefunction which solves this equation is

$$\psi = \psi_0 \exp\left(i\frac{e}{\hbar c}\int_s \mathbf{A}\cdot\mathbf{dl}\right), \tag{2}$$

where $\psi_0(\mathbf{r},t)$ is the solution for the unperturbed equation of motion with $\mathbf{A}=0$, and the integral is taken along a trajectory of the particle in space. When the path is closed, a gauge-independent relative phase ensues between the encircling wavepackets, known as the Aharonov-Bohm phase. If the vector potential $\mathbf{A}$ changes in time, it leads to the time-dependent Aharonov-Bohm effect, where the trajectory is taken over space and time [41–43].

II. THE TEMPORAL AHARONOV-BOHM EFFECT

We adapt the time-dependent spatial Aharonov-Bohm effect to the time domain by considering the dispersion of pulses in time, up to the third order [44]:

$$\frac{\partial u(t,z)}{\partial z} = -\frac{i}{2}\beta_2\frac{\partial^2 u(t,z)}{\partial t^2} - \beta_1\frac{\partial u(t,z)}{\partial t} + i\beta_0 u(t,z), \tag{3}$$

where $u(t,z)$ is the pulse envelope. Since β_0 is a gauge field, this can be reordered as

$$\frac{\partial u(t,z)}{\partial z} = -i\left(\beta_A\frac{\partial}{\partial t} + i\beta_B\right)^2 u(t,z), \tag{4}$$

*Contact author: mordechai.fridman@biu.ac.il

Published by the American Physical Society under the terms of the Creative Commons Attribution 4.0 International license. Further distribution of this work must maintain attribution to the author(s) and the published article's title, journal citation, and DOI.

where $\beta_A = \sqrt{\beta_2/2}$ and $\beta_B = -\beta_1/\sqrt{2\beta_2}$ are the dispersion relations. This equation is the temporal equivalent of Eq. (1), hence the solution is

$$u(z) = u(0)\exp\left(-i\int_s \frac{\beta_1(z,t')}{\beta_2(z,t')}dt'\right), \tag{5}$$

where the integral is taken along a trajectory in the two-dimensional space spanned by the time and propagation axes. We compare the phases accumulated from two distinct spatiotemporal paths and interpret the difference between these phases as the temporal Aharonov-Bohm effect. In the standard Aharonov-Bohm effect, the phase of the particle is sensitive to the vector potential even when the particle traverses a field-free region. In our temporal Aharonov-Bohm system, the phase is sensitive to changes in β_1 or β_2 even when the photons' temporal paths are in constant β_1 and β_2 regions. Detailed derivation leading to Eqs. (4) and (5) is shown in Sec. S1.1 in the Supplemental Material [45].

III. EXPERIMENTAL SETUP

To demonstrate the temporal Aharonov-Bohm system, and allow for increased phase sensitivity, we employ our temporal SU(1,1) interferometer [25] by tuning the pumps timing. The temporal SU(1,1) interferometer has two time lenses in a series, each generates an idler beam along with the signal. This idler beam is proportional to the Fourier transform of the input signal. As a result, at the output signal and idler there is an interference between two modes from the two time lenses. The resulting output idler is the interference between a beam that is generated in the first time lens and another that is generated in the second (the resulting output signal is the interference between a beam that is generated by the first time lens and generated again by the second, and another beam that only passes through the two time lenses).

In our case, since the signal and idler are in Fourier relations, we choose a Gaussian-shaped input signal leading to similar temporal shapes of the signal and idler outputs [25], as shown in detail in Sec. S1.2 in the Supplemental Material. We also extend the temporal SU(1,1) into a temporal 8f configuration, where each time lens is at an imaging condition with $M = -1$ magnification, and therefore, the outputs of the signal and idler have similar temporal shapes for symmetric inputs which are non-Gaussian, as shown in detail in Sec. S2.2 in the Supplemental Material [45].

We present the temporal Aharonov-Bohm system in Fig. 1(b) as a temporal ray scheme, by replacing space with time [46–50], while our point of reference moves with the pump wavelength. The signal and idler modes propagate along the fiber at different velocities due to dispersion. In this temporal ray scheme, we denote the signal and idler by red and blue curves, respectively, moving in the positive and negative directions with respect to the pump. The two modes have different temporal paths, while encircling a spatiotemporal area. The two modes accumulate the phase along their paths, according to Eq. (5), leading to an equivalence to the Aharonov-Bohm effect in the time domain. A simplified scheme of the experimental setup is shown in Fig. 1(a). The signal enters the first time lens and stimulates the generation of a signal-idler pair by a nonlinear interaction with a chirped

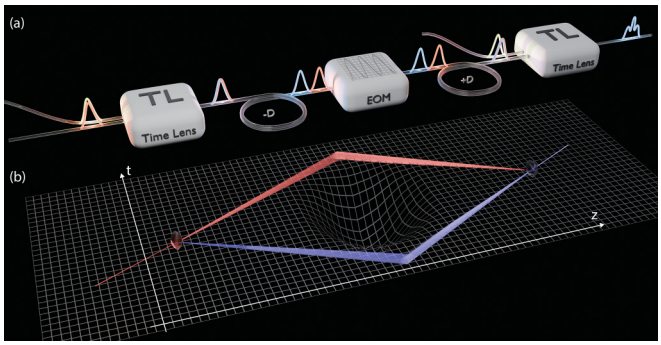


FIG. 1. (a) Block diagram of the experimental setup of temporal Aharonov-Bohm system. (b) Illustration of the temporal Aharonov-Bohm effect. The signal enters the first time lens and stimulates the generation of a signal-idler pair. Both modes encircle a spatiotemporal region, experience a nonzero potential, and interfere in the second time lens.

pump. The signal and idler propagate along a dispersive fiber, opening a gap of 67 ps between them. An electro-optic modulator (EOM) is situated at the Fourier plane, where they have similar temporal shapes. The signal and idler probe the phase of the EOM at different timings with a temporal separation of 67 ps. Next, they propagate along a dispersion compensating fiber, so the temporal gap between them closes. Then, they enter the second time lens where they interact with another chirped pump. The second time lens generates new signal and idler modes, that interfere with the original modes. Details and schematic of the experimental setup are shown in Sec. S2.1 in the Supplemental Material [45].

To demonstrate the influence of the Aharonov-Bohm effect, we impose a sinusoidal phase change by the EOM. The EOM changes the dispersion components β_1 and β_2 as a function of time. This change in dispersion as a function of time is equivalent to the standard Aharonov-Bohm effect, where the potential changes as a function of space. Since the EOM is localized at a single point along the propagation axis, the path integral in Eq. (5) depends only on time. Moreover, since the duration of our signal pulse is orders-of-magnitude-smaller than the period time of the EOM, the path integral reduces to $\beta_1(t)/\beta_2(t)$, and therefore the solution after neglecting a constant phase resulting from the integral is

$$u(t) = u(0)\exp\left(-i\frac{\beta_1(t)}{\beta_2(t)}\Delta t\right) \approx u(0)\exp\left(i\omega_{\mathrm{EOM}}t\right), \tag{6}$$

where ω_{EOM} is the modulating frequency of the EOM and we assume $\omega_{\mathrm{EOM}}t \ll 1$. Therefore, the temporal fringes pattern of the idler follows

$$I_i(t) \propto \cos\left((2ab - \omega_{\mathrm{EOM}})t\right)\exp\left(-\frac{1}{2}\frac{t^2}{\phi_p''^2}\sigma^2\right), \tag{7}$$

where a is set by tuning the dispersion in the system, b is set by tuning the relative timing between the pumps, ϕ_p'' is the group delay dispersion (GDD) of the pump, and σ is the input signal temporal width. The detailed analytic derivation is shown in Sec. S1.3 in the Supplemental Material [45].

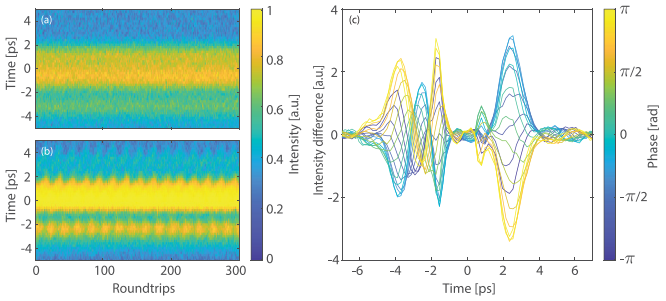


FIG. 2. (a) Idler output when the EOM is not oscillating. (b) Idler output when the EOM is oscillating in 4 GHz. The output idler has a fringe pattern that shifts periodically in time. (c) Idler fringes which are obtained from different phases of the EOM period for EOM frequency of 4 GHz and amplitude of 13 dBm. The fringe periodicity is 2.8 ps.

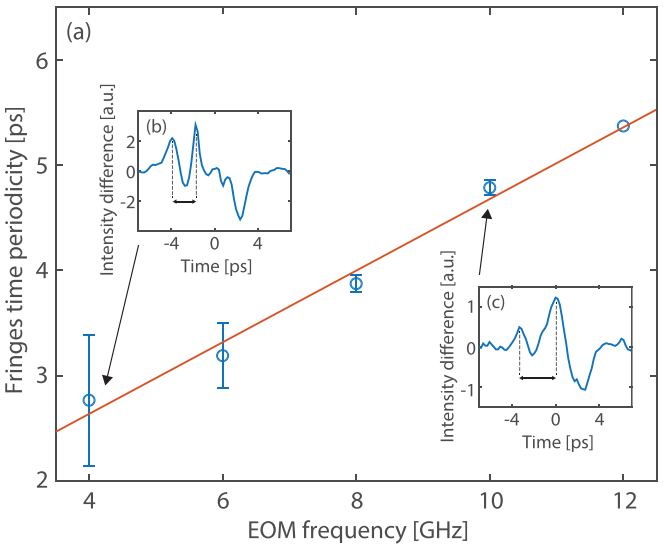


FIG. 3. (a) Periodicity of the output idler fringes as a function of the EOM frequency, at EOM amplitude of 13 dBm. The periodicity increases along with the EOM frequency, with a linear fit. (b) Representative periodicity for EOM frequency of 4 GHz, with average periodicity of 2.8 ps. (c) Representative periodicity for EOM frequency of 10 GHz, with average periodicity of 4.8 ps.

IV. INTERFERENCE MEASUREMENTS

We demonstrate the ability of the Aharonov-Bohm system to measure fast phase changes as a function of time, and to determine the EOM frequency. We set the frequency range of the EOM to 4–12 GHz, and measure the temporal fringes of the output idler from the Aharonov-Bohm system. We tune the temporal shift between the two pumps to ensure that the system is sensitive to an EOM frequency range of 4–12 GHz. Hence, the fringes are not too dense for our resolution threshold of 0.5 ps, and are not too spacious for our signal temporal width of 12 ps.

We compare the output idler of the Aharonov-Bohm system when the EOM is not oscillating [Fig. 2(a)], and when the EOM is oscillating at 4 GHz [Fig. 2(b)]. When the EOM is oscillating, we observe fringes that periodically shift between roundtrips. Although we are not locking the EOM phase to the repetition rate of the laser, we are measuring over 50 000 different measurements so we are sampling the EOM in all its possible phases. These fringes become stationary when the EOM is not oscillating, indicating that our Aharonov-Bohm system is indeed affected by the EOM.

We focus on a single period of the EOM and measure the temporal fringes in the output idler. As the signal and idler encounter the EOM at different timings, they exhibit different phases in a periodic pattern. We subtract the mean intensity of all the roundtrips to remove the bias and average over 5000 measurements. The output idler is shown in Fig. 2(c) where the fringes obtained from different phases of the EOM period are denoted by the color bar, for a 4 GHz frequency of the EOM. Thus, we demonstrate the temporal fringes as a function of the EOM phases with a fringe periodicity of 2.8 ps.

Next, we measure the fringe periodicity as a function of the EOM frequency, shown in Fig. 3. Representative results of the periodicity of the output for 4 GHz and 10 GHZ are shown in the insets. The fringe periodicity grows with the EOM frequency. Due to experimental difficulties, we were unable to obtain enough data points for a reliable error bar at 12 GHz frequency of the EOM. Nevertheless, the periodicity of the fringes increases monotonically with a linear fit $R^2 = 0.99$. This linear relation between the periodicity of the fringes and the EOM frequency allows us to quantitatively identify temporal phase changes in the system. The fringe periodicity follows $2ab - \omega_{\mathrm{EOM}}$ in Eq. (7). Thus, the fringe periodicity increases as ω_{EOM} increases.

V. DEMONSTRATION OF QUANTUM-ENHANCED SENSITIVITY

To assess the sensitivity of the system, we decrease the EOM amplitude from 15 dBm down to 1 dBm and measure the signal-to-noise ratio (SNR) of the output idler. The fringes pattern fades as we reduce the EOM amplitude and the SNR decreases, respectively, as shown in Figs. 4(a) and 4(b), denoted by the blue triangles for 4 GHz and 10 GHz, respectively. We observe that the SNR increases with the EOM amplitude ranging between two for low amplitude and ten for high amplitude.

We utilize the correlation between the signal and idler modes to increase the system's sensitivity [51]. Since the signal and idler are generated by the four-wave mixing (FWM) process in the first time lens, they are correlated during their spatiotemporal paths. We improve the sensitivity by evaluating the joint temporal function (JTF) between the signal and idler outputs [49]. This is obtained by summing over the temporal correlations of many measured signal and idler outputs. The JTF is similar to calculating the joint spectral function, with measuring the temporal correlation instead of the spectral correlation. Due to the phase from the temporal Aharonov-Bohm effect, we observe an interference pattern in the JTF [49]. The JTF has higher sensitivity and is less affected by noise since the noise generates uncorrelated photons while the JTF corresponds to correlated photons, as analytically shown in Sec. S1.4 in the Supplemental Material [45].

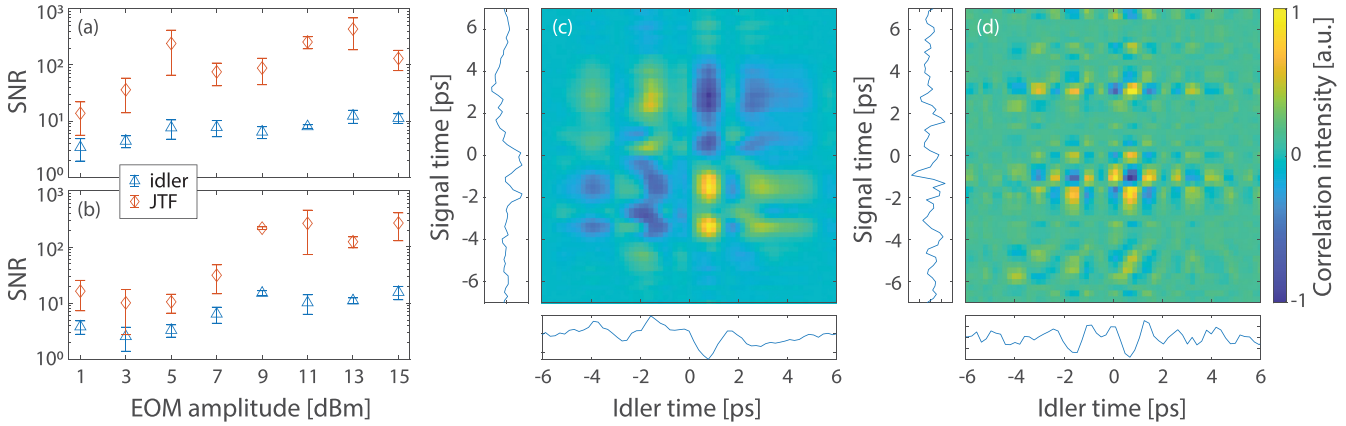


FIG. 4. (a), (b) Comparison between SNR of the output idler (blue triangle), and the SNR of the temporal correlation between the outputs signal and idler (orange diamond) for 4 GHz and 10 GHz resonance frequencies of the EOM, respectively. By utilizing the temporal SU(1,1) to measure the phase of the Aharonov-Bohm effect, we get higher sensitivity. (c) JTF of the output signal and idler by applying EOM frequency of 4 GHz. This JTF has a chessboard pattern with a diagonal shape, indicating a high correlation between the modes regardless of the low EOM amplitude. (d) JTF of the two outputs by applying 10 GHz resonance frequency of the EOM. This JTF has a denser pattern, indicating the higher frequency.

For each phase of the EOM period, we evaluate the JTF as an outer product between the output signal and idler and sum all the outer products. In Figs. 4(c) and 4(d), we show the JTFs of the output signal and idler for EOM frequencies of 4 GHz and 10 GHz, respectively, where the EOM amplitude is set to 3 dBm. Representative signal and idler for one phase of the EOM are shown next to each, Figs. 4(c) and 4(d). As evident, Fig. 4(c) shows a chessboard pattern with a diagonal shape, indicating a high correlation between the modes regardless of the low EOM amplitude. Figure 4(d) shows a denser chess pattern due to the higher EOM frequency agreeing with the calculated JTF in Sec. S1.4 in the Supplemental Material [45].

We evaluate the SNR of the JTF as the ratio between the peak power of the JTF and the maximum power of the noise. We show the SNR of the JTF for 4 GHz and 10 GHz in Figs. 4(a) and 4(b), respectively, denoted by the red diamonds. As evident, the SNR of the JTS is higher compared to the SNR of the idler alone, denoted by the blue triangles. We obtain an improvement of up to a factor of 50 with the JTF, achieved by the quantum properties of the SU(1,1) interferometer and the use of entangled photons [25].

VI. DISCUSSION

To conclude, we proposed and experimentally analyzed a temporal Aharonov-Bohm system, while demonstrating its ability to measure fast phase changes. Our method's sensitivity is enhanced by exploiting the quantum properties of a temporal SU(1,1) interferometer, thereby utilizing entangled states of light and the strong correlations they enable. This temporal Aharonov-Bohm system can revolutionize the field of optical spatiotemporal dynamics, offering high temporal resolution through single-shot measurements with sensitivity surpassing, in principle, the shot-noise limit. This is a demonstration of Aharonov-Bohm effect in the time domain and a demonstration of the Aharonov-Bohm effect with entangled particles. Our temporal Aharonov-Bohm system is suitable for analyzing systems, where the dispersion changes rapidly as a function of space and time. In addition to the interest in adapting this quantum phenomenon to the time domain, it can improve quantum-enhanced measurements [26–28], metrology at GHz frequencies [29,30], advanced sensing of dispersion properties [31,32], and high-precision temporal measurements [33]. Also, by developing this system for ultrafast phase dynamics, it will be relevant for simulation applications, where the optical properties change in space and time, or those involving the generation of entangled modes, such as optical analogs of rotating black holes, where the index of refraction is equivalent to the curvature of spacetime [35–38], Thomas precession [39], gravitational frame dragging [34], and redshift effects [34].

ACKNOWLEDGMENTS

The research was funded by the Israel Science Foundation, Grants No. 2942/24 and No. 2208/24, and by the European Union's Horizon Europe research and innovation programme, Grant No. 101178170.

[1] Y. Aharonov and D. Bohm, Significance of electromagnetic potentials in the quantum theory, Phys. Rev. **115**, 485 (1959).

[2] Y. Aharonov and D. Bohm, Further considerations on electromagnetic potentials in the quantum theory, Phys. Rev. **123**, 1511 (1961).

[3] M. Peshkin and A. Tonomura, *The Aharonov–Bohm Effect* (Springer, Berlin, 1989).

[4] Y. Aharonov, E. Cohen, and D. Rohrlich, Nonlocality of the Aharonov-Bohm effect, Phys. Rev. A **93**, 042110 (2016).

[5] L. Vaidman, Role of potentials in the Aharonov-Bohm effect, Phys. Rev. A **86**, 040101(R) (2012).

[6] Y. Aharonov, E. Cohen, and D. Rohrlich, Comment on "Role of potentials in the Aharonov-Bohm effect", Phys. Rev. A **92**, 026101 (2015).

[7] M. V. Arkhipov, R. M. Arkhipov, and N. N. Rosanov, Optical Aharonov—Bohm effect, JETP Lett. **111**, 668 (2020).

[8] C. Tan, The Berry phase and the Aharonov-Bohm effect on optical activity, Opt. Express **16**, 14675 (2008).

[9] C. Tan, Aharonov–Bohm effect in optical activity, J. Phys. A: Math. Theor. **43**, 354007 (2010).

[10] A. Govorov, S. Ulloa, K. Karrai, and R. Warburton, Polarized excitons in nanorings and the optical Aharonov-Bohm effect, Phys. Rev. B **66**, 081309(R) (2002).

[11] R. J. Cook, H. Fearn, and P. W. Milonni, Fizeau's experiment and the Aharonov–Bohm effect, Am. J. Phys. **63**, 705 (1995).

[12] A. Besharat, M. Miri, and M. Nouri-Zonoz, Optical Aharonov–Bohm effect due to toroidal moment inspired by general relativity, J. Phys. Commun. **3**, 115019 (2019).

[13] D. Neshev, A. Nepomnyashchy, and Y. S. Kivshar, Nonlinear Aharonov-Bohm scattering by optical vortices, Phys. Rev. Lett. **87**, 043901 (2001).

[14] S. A. Werner and A. G. Klein, Observation of Aharonov–Bohm effects by neutron interferometry, J. Phys. A: Math. Theor. **43**, 354006 (2010).

[15] Y. Aharonov and A. Casher, Topological quantum effects for neutral particles, Phys. Rev. Lett. **53**, 319 (1984).

[16] C. Overstreet, P. Asenbaum, J. Curti, M. Kim, and M. A. Kasevich, Observation of a gravitational Aharonov-Bohm effect, Science **375**, 226 (2022).

[17] M. Anacleto, I. Salako, F. Brito, and E. Passos, Analogue Aharonov-Bohm effect in neo-Newtonian theory, Phys. Rev. D **92**, 125010 (2015).

[18] C. Dartora, K. Nobrega, and G. Cabrera, Optical analogue of the Aharonov–Bohm effect using anisotropic media, Phys. Lett. A **375**, 2254 (2011).

[19] L. R. Jaroszewicz, Z. Krajewski, and L. Solarz, Absolute rotation measurement based on the Sagnac effect, in *Earthquake Source Asymmetry, Structural Media and Rotation Effects*, edited by R. Teisseyre, E. Majewski, and M. Takeo (Springer, Berlin, Heidelberg, 2006), pp. 413–438.

[20] E. J. Post, Sagnac effect, Rev. Mod. Phys. **39**, 475 (1967).

[21] R. Wang, Y. Zheng, and A. Yao, Generalized Sagnac effect, Phys. Rev. Lett. **93**, 143901 (2004).

[22] E. Li, B. J. Eggleton, K. Fang, and S. Fan, Photonic Aharonov–Bohm effect in photon–phonon interactions, Nat. Commun. **5**, 3225 (2014).

[23] K. Fang, Z. Yu, and S. Fan, Photonic Aharonov-Bohm effect based on dynamic modulation, Phys. Rev. Lett. **108**, 153901 (2012).

[24] N. Satapathy, D. Pandey, P. Mehta, S. Sinha, J. Samuel, and H. Ramachandran, Classical light analogue of the non-local Aharonov-Bohm effect, Europhys. Lett. **97**, 50011 (2012).

[25] S. Meir, Y. Tamir, H. Duadi, E. Cohen, and M. Fridman, Ultrafast temporal SU(1,1) interferometer, Phys. Rev. Lett. **130**, 253601 (2023).

[26] M. Genovese, Experimental quantum enhanced optical interferometry, AVS Quantum Sci. **3**, 044702 (2021).

[27] D. Salykina and F. Khalili, Sensitivity of quantum-enhanced interferometers, Symmetry **15**, 774 (2023).

[28] M. D. Lang and C. M. Caves, Optimal quantum-enhanced interferometry, Phys. Rev. A **90**, 025802 (2014).

[29] A. Cabral and J. Rebordão, Accuracy of frequency-sweeping interferometry for absolute distance metrology, Opt. Eng. **46**, 073602 (2007).

[30] A. Cabral and J. Rebordao, Absolute distance metrology with frequency sweeping interferometry, in *Recent Developments in Traceable Dimensional Measurements III* (SPIE, San Diego, California, 2005), Vol. 5879, pp. 195–204.

[31] S. P. Velsko and D. Eimerl, Precise measurements of optical dispersion using a new interferometric technique, Appl. Opt. **25**, 1344 (1986).

[32] X. Lou, Y. Wang, and Y. Dong, Multipoint dispersion spectroscopic gas sensing by optical FMCW interferometry, Opt. Lett. **46**, 5950 (2021).

[33] Y. Zhang, Z. Zeng, L. Zhang, X. Zou, F. Yang, Z. Zhang, S. Zhang, H. Li, and Y. Liu, Ultrafast and high-precision time delay measurement based on complementary frequency-swept light and frequency-shifted dechirping, J. Lightwave Technol. **42**, 1927 (2023).

[34] U. Leonhardt, Casimir cosmology, Int. J. Mod. Phys. A **37**, 2241006 (2022).

[35] M. Cromb, G. M. Gibson, E. Toninelli, M. J. Padgett, E. M. Wright, and D. Faccio, Amplification of waves from a rotating body, Nat. Phys. **16**, 1069 (2020).

[36] I. Brevik and G. Halnes, Light rays at optical black holes in moving media, Phys. Rev. D **65**, 024005 (2001).

[37] J. Drori, Y. Rosenberg, D. Bermudez, Y. Silberberg, and U. Leonhardt, Observation of stimulated hawking radiation in an optical analogue, Phys. Rev. Lett. **122**, 010404 (2019).

[38] D. Faccio, T. Arane, M. Lamperti, and U. Leonhardt, Optical black hole lasers, Class. Quantum Grav. **29**, 224009 (2012).

[39] D. Han, E. E. Hardekopf, and Y. S. Kim, Thomas precession and squeezed states of light, Phys. Rev. A **39**, 1269 (1989).

[40] A. Retzker, Y. Aharonov, A. Botero, S. Nussinov, and B. Reznik, Aharonov-Bohm effect without closing a loop, Phys. Rev. A **73**, 032106 (2006).

[41] D. Singleton and E. C. Vagenas, The covariant, time-dependent Aharonov–Bohm effect, Phys. Lett. B **723**, 241 (2013).

[42] M. Bright and D. Singleton, Time-dependent non-Abelian Aharonov-Bohm effect, Phys. Rev. D **91**, 085010 (2015).

[43] K. Ma, J.-H. Wang, and H.-X. Yang, Time-dependent Aharonov–Bohm effect on the noncommutative space, Phys. Lett. B **759**, 306 (2016).

[44] G. P. Agrawal, Nonlinear fiber optics, in *Nonlinear Science at the Dawn of the 21st Century*, edited by P. L. Christiansen, M. P. Sorensen, and A. C. Scott (Springer, Berlin, 2000), pp. 195–211.

[45] See Supplemental Material at http://link.aps.org/supplemental/10.1103/3phs-9rmc for a detailed derivation of the analytical expressions and discuss technical details related to the experimental setup.

[46] A. Klein, I. Sibony, S. Meir, S. Shahal, H. Duadi, and M. Fridman, Overlapping time-lens array, IEEE Photon. J. **11**, 1 (2019).

[47] A. Klein, I. Sibony, S. Meir, H. Duadi, M. Y. Sander, and M. Fridman, Temporal imaging with a high filling factor, APL Photonics **5**, 090801 (2020).

[48] Y. Zhang, C. Tao, S. Luo, K. Y. Lau, J. Zheng, L. Huang, A. Zhang, L. Sheng, Q. Ling, Z. Guan *et al.*, Ultra-fast optical time-domain transformation techniques, Nat. Rev. Methods Primers **5**, 11 (2025).

[49] S. Meir, A. Klein, H. Duadi, E. Cohen, and M. Fridman, Single-shot analysis of amplified correlated light, Opt. Express **30**, 1773 (2022).

[50] A. Klein, S. Shahal, S. Meir, H. Duadi, K. Sulimany, O. Lib, H. Steinberg, S. A. Kolpakov, and M. Fridman, Ultrafast twin-peak rogue waves in a vector field, OSA Continuum **2**, 3102 (2019).

[51] P. Samuelsson, E. V. Sukhorukov, and M. Büttiker, Two-particle Aharonov-Bohm effect and entanglement in the electronic hanbury Brown–Twiss setup, Phys. Rev. Lett. **92**, 026805 (2004).